CHAPTER 1
Introduction
CHAPTER 2
Machining Dynamics
CHAPTER 3
Robust Control Approach

ลิขสิทธิ์มหาวิทยาลัยเชียงใหม่
Copyright© by Chiang Mai University
All rights reserved

CHAPTER 4

Hardware-in-the-Loop Test System for Machining Emulation

4.1 Active Control Architecture

The test system used for this study has been designed to emulate a milling operation with active control hardware. For a standard machine spindle configuration, both ends of the spindle will be supported by ball bearings as shown in Figure 4.1(a). To create an active structure, a magnetic bearing or bearing actuator may be used, as shown in Figure 4.1(b) and (c). Such active bearing elements have been used previously in chatter control research studies [88], [19], [71]. With this approach, the structural dynamics will involve the effect from spindle and tool flexibility and this must be accounted for in chatter prediction and control. For a typical spindle structure supported by magnetic bearings there may be major modes associated with rigid body motion and additional modes associated with flexibility of the tool and/or spindle shaft [31]. For this thesis, a mock-up of a machine spindle with a single active magnetic bearing has been developed. The concept for the test system is shown in Figure 4.1(d).

The test system used for experimental study is shown in Figure 4.2. The structure has been designed to exhibit two main resonances and is dynamically similar to an AMB-supported milling spindle that exhibits significant cutting tool flexibility [28]-[33]. The main structure is a flexure-pivoted beam connected to an end-mass through another flexure pivot. Two non-contact electromagnetic actuators (1-D active magnetic bearings) are used to apply forces to the structure.

Hardware-in-the loop simulation and controller testing for machining vibration can be undertaken based on the configuration shown in the block diagram Figure 4.3. In this scheme, actuator 2 is an auxiliary actuator used to apply the simulated cutting force that is computed in real-time using a cutting force model implemented within the control hardware. This also requires real-time measurement of the 'tool' displacement.

ลิขสิทธิ์มหาวิทยาลัยเชียงใหม่
Copyright© by Chiang Mai University
All rights reserved

Actuator 1 is the control actuator and is used to apply the stabilizing control forces. Note that, as the cutting force model is implemented digitally on the control hardware, the cutting model can be selected freely, subject to limits of actuator force capacity and bandwidth.

Displacement of the structure can be measured by two non-contact (eddy current) sensors positioned close to the actuators. Additional vibration measurements were obtained using strain gauges at the flexure locations. Displacement measured directly at the cutting location was used for calculation of the simulated cutting force but was not used for feedback. In practice, it may be difficult to obtain such measurement on a real system and therefore the controller designs are based on direct measurements of the spindle deflection away from the tool tip. For a fourth order (two-mode) model, full state information may be obtained by combined use of the displacement and strain sensors located away from the 'tool' end.

The spindle structure design was made such that the dominant natural frequencies were in a low frequency range (not exceed $0-200$ Hz). This is done to allow closed-loop control within the bandwidth of the actuators and with practically low sampling frequencies (1000-5000 Hz) for the digital control implementation. The resonance frequencies for the other parts on the test system such as the base frequency, sensor leg stations and especially the unmodelled structure modes, etc, are significantly higher.

The basic concept for operation of the test system is shown in Figure 4.3. The external forces that act on the spindle structure are

ลิขสิทธิ์มหาวิทยาลัยเชียงใหม่
Copyright© by Chiang Mai University
All rights reserved

1) Input control force u (actuator 1): This is the active control force which is determined by the feedback control algorithm. Initially, a local PD control force is applied to stabilize the system and this is also the base-level control that will be used as a benchmark for comparing the stability/performance of designed controllers.

2) Simulated cutting force w (actuator 2): This force is the virtual cutting force that allows the effects of the cutting force to be replicated. By using feedback of the measured displacement y_t it is possible to choose the force to match the cutting force model in (2.5).

The measured signals used in this study were requires to include the vibration displacement of the spindle and the cutting tool. Due to lack of space to install the displacement sensors (see Figure 4.2) it is possible instead to calculate the output signals for displacement at actuator 1 and 2, (y_a and y_t) by using the measurement signals, y_a^m, y_{t1}^m, y_{t2}^m and ε as shown in Figure 4.4 by assuming a linear relationship:

i) For the vibration displacement of the spindle at actuator 1,

$$y_a = \kappa_a y_a^m \tag{4.1}$$

where y_a^m is the directly measured signals and κ_a is a constant values which determined by similar triangles rule based on the motion being a fixed pivot at the base flexure.

ii) The displacement vibration of spindle at actuator 2 (cutting tool displacement) may be approximated as follows

$$y_t = 0.5\left(y_{t1}^m + y_{t2}^m\right). \tag{4.2}$$

Where the middle distance between the sensors signal y_{t1}^m and y_{t2}^m is co-location to the cutting force location. In actual cutting, it is difficult to directly measure the cutting tool displacement vibration due to the cutting tool is immersion in the workpiece. So then, to obtain y_t in a more realistic setting, the signals from the strain gauges at flexure pivot 2 can be used to estimate y_t, gain by using a linear form which also involves y_a as follows:

$$y_t = y_a + \kappa_\varepsilon \varepsilon + c_\varepsilon \tag{4.3}$$

where κ_ε is a strain gauge contribution coefficient and c_ε is an adjusted offset value. The values of these parameters were set manually so that the displacement estimate using the strain gauge signal matched the displacement signal from direct measurement.

ลิขสิทธิ์มหาวิทยาลัยเชียงใหม่
Copyright© by Chiang Mai University
All rights reserved

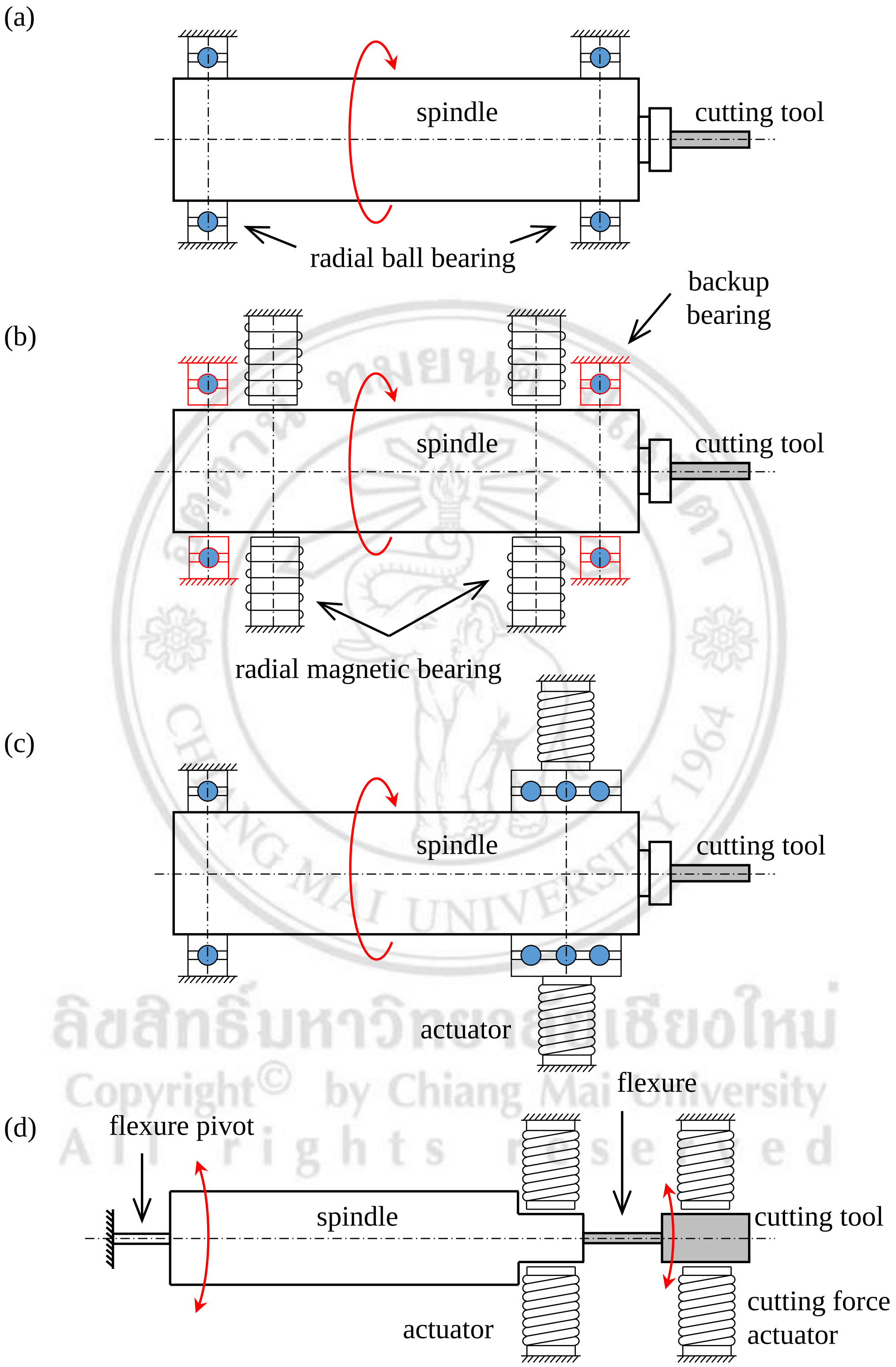

Figure 4.1 Illustration of milling machine configurations with different types of support (a) radial ball bearing, (b) AMBs, (c) radial ball bearings with actuator [16], [71], (d) test system structure supported by flexure pivot and electromagnetic actuator.

ลิขสิทธิ์มหาวิทยาลัยเชียงใหม่
Copyright© by Chiang Mai University
All rights reserved

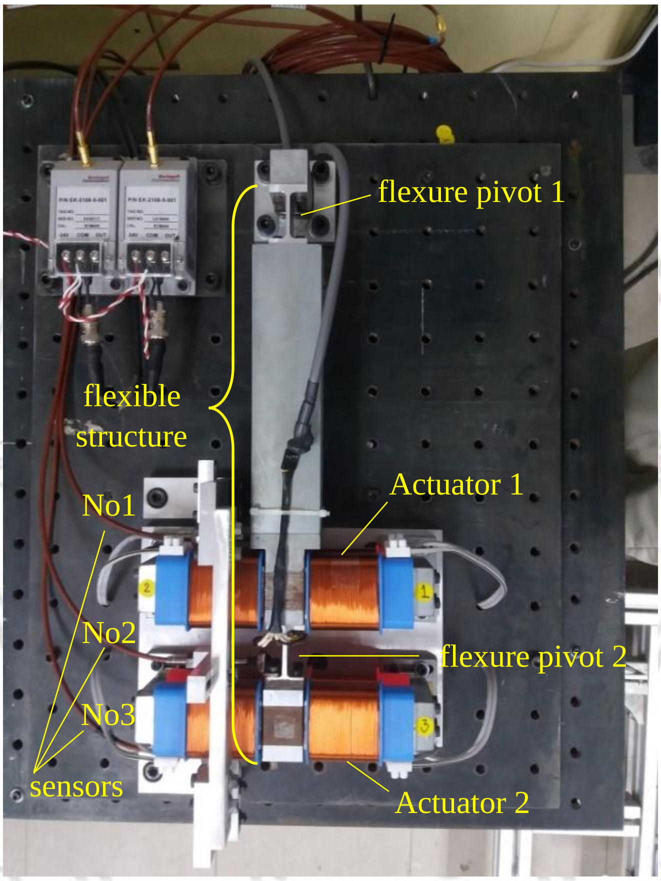

ลิขสิทธิ์มหาวิทยาลัยเชียงใหม่
Copyright© by Chiang Mai University
All rights reserved

Figure 4.2 Main components of test system for experiments on active vibration control of machine structures.

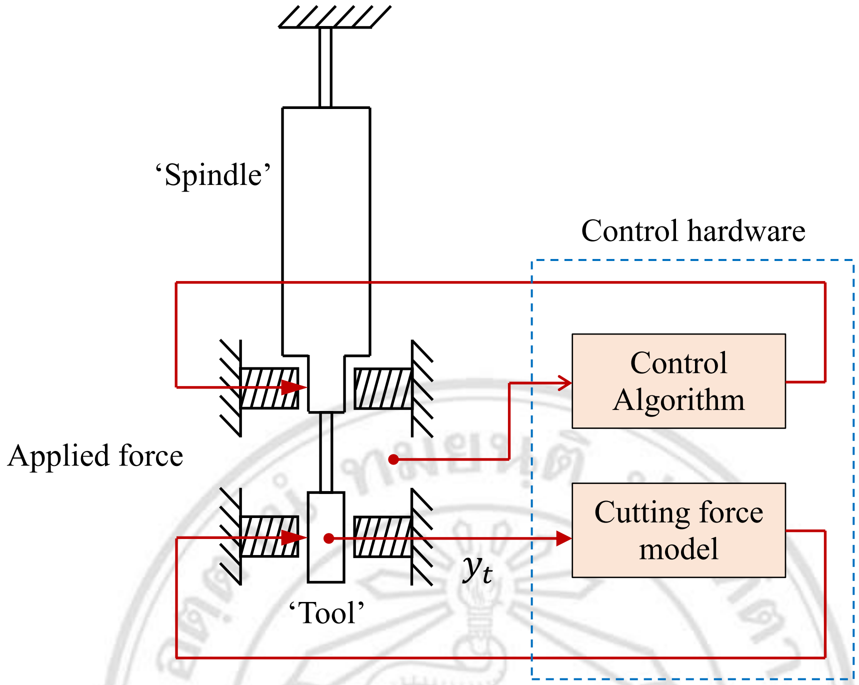

Figure 4.3 Operating principle of test system for experiments on active vibration control of machine structures.

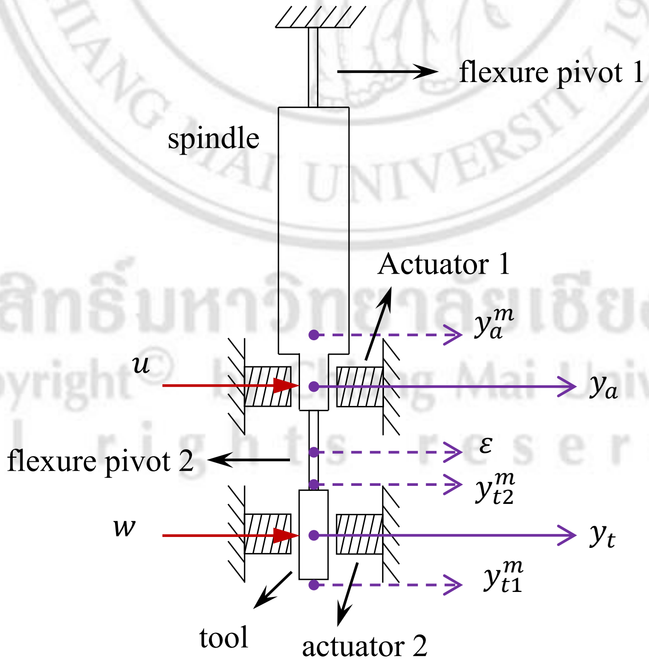

Figure 4.4 Test system concept and input/output measurement signals representations.

ลิขสิทธิ์มหาวิทยาลัยเชียงใหม่
Copyright© by Chiang Mai University
All rights reserved

4.2 Test System Flexible Structure

The test system flexible structure has a number of sections with different rectangular cross sections as shown in Figure 4.5. Steel with zinc coating for anti-corrosion is used for the main section (B) to represent a machining spindle rotor. To ensure good force transmissions and reduce eddy-current losses when applying magnetic forces from actuators, two laminated stack sheets, (D1) and (D2), are used. The actuators installed at these locations provide stabilizing control force and emulated cutting force respectively. The main structures (B) and (D) are connected by aluminium flexures (A) and (C). The flexure (A) represents a pivot point supported by a ball bearing while the flexure (C) represents a flexible cutting tool. Strain gauges with bridge circuit are installed on the flexure (C) as shown in Figure 4.6 to provide an additional strain measurement for the feedback controller.

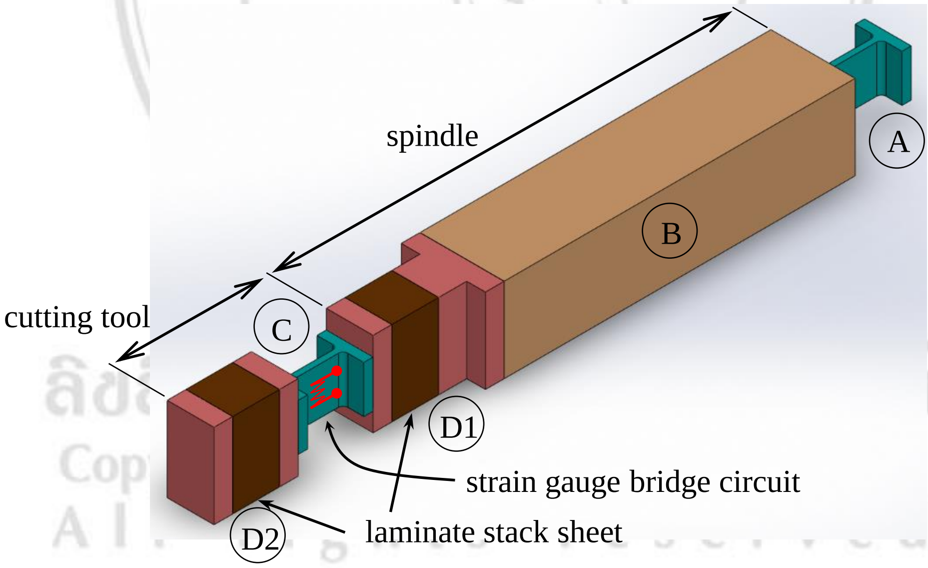

Figure 4.5 Test system flexible structure assembly detail

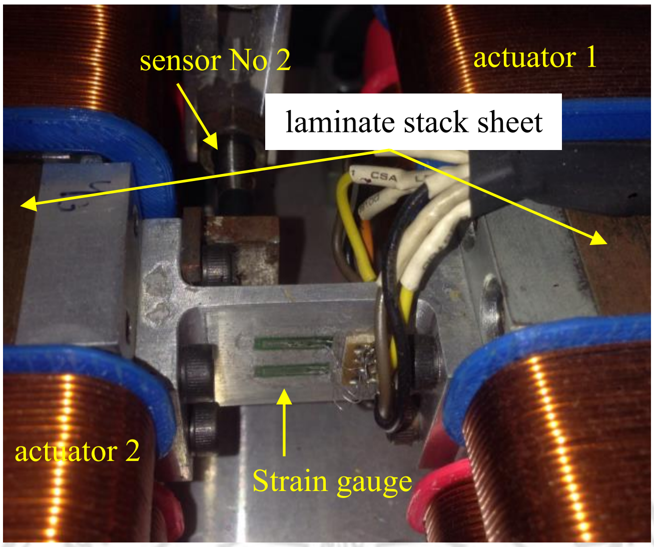

Figure 4.6 Close-up view of strain gauge bridge circuit

4.3 Actuators

The actuator 1 and 2 have the same structure and size and only differ in purpose of use: actuator 1 is used for active control of the induced vibration in the test system structure and actuator 2 is the cutting force generator, as shown in Figure 4.7. The operating principle of the actuator is to convert the electrical energy to mechanical energy. It consists of electromagnetic units, power amplifiers and a controller unit as shown in Figure 4.8. The controller unit could use the displacement signals from the eddy current sensors and strain gauge to determine the control signals and transmits these signals to the power amplifiers. The electric control current from the amplifier supplying to the electromagnet coil generates a magnet field that causes an attracting force on the laminated stack sheet within the structure (see Figure 4.5).

The magnetic coils are driven by pulse-width modulation (PWM) switching amplifiers from Copley Corporation Corp and operate with bias current of 1.5 Amp. In order to cancel the negative stiffness of the electromagnet, localized PD control feedback is implemented. This allows the actuator to be modelled as a neutral but lightly damped support. Additional control forces from other active controller designs can be applied by superposition with the PD feedback control signals.

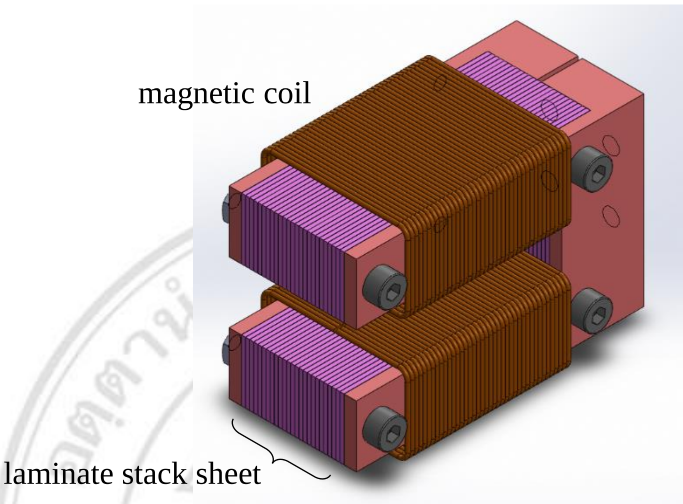

Figure 4.7 Actuator detail

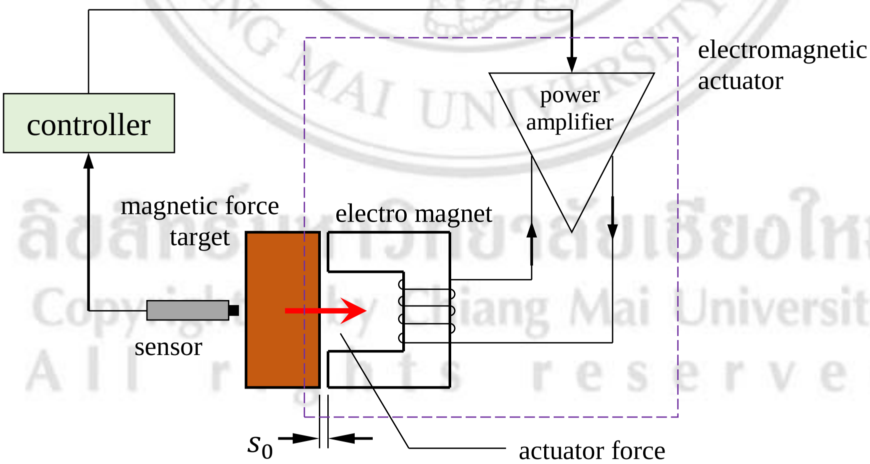

Figure 4.8 Actuator control concept

ลิขสิทธิ์มหาวิทยาลัยเชียงใหม่
Copyright© by Chiang Mai University
All rights reserved

4.3.1 Actuator model

With appropriated bias currents, the linearized model of actuator force can be described as [88]

$$f_A(y,i) = k_i i - k_s y \tag{4.4}$$

where i is the coil current and y is the size of the gap between the actuator and target. The constant k_i (N/Amp) is the *force/current factor* and k_s (N/m) is the *force/displacement factor* (This factor is commonly called the actuator negative stiffness).

In order to obtain (4.4), the total actuator force acting on the flexible structure is generated by two counteracting magnets as shown in Figure 4.9. This configuration makes it possible to generate both positive and negative magnetic forces in a *differential driving mode*. In this mode, one magnet coil is driven with the sum of bias current i_0 and control current i, $(i_0 + i)$, and the other one is driven with the difference of these currents, $(i_0 - i)$. The sum of these two opposing magnetic forces with the

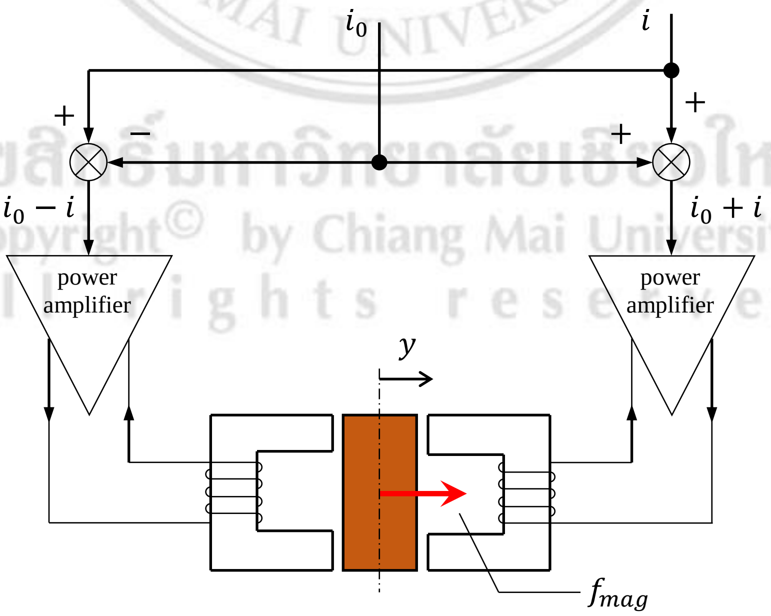

Figure 4.9 Differential driving mode of the actuator

ลิขสิทธิ์มหาวิทยาลัยเชียงใหม่
Copyright© by Chiang Mai University
All rights reserved

corresponding air gaps, $(s_0 + y)$ and $(s_0 - y)$ can be written as

$$f_A = f_+ - f_- = k\left(\frac{(i_0+i)^2}{(s_0-y)^2} - \frac{(i_0-i)^2}{(s_0+y)^2}\right) \tag{4.5}$$

where $k = \frac{1}{4}\mu_0 n^2 A_a$ ($\mu_0 = 4\pi\times10^{-7}$ Vs/Am), n is a number of turns in the magnetic coil and A_a is a cross-section area of the air gap. Then, the linearization of (4.5) about $y = 0$ with respect to y is

$$f_A = \frac{4ki_0}{s_0^2}i - \frac{4ki_0^2}{s_0^3}y = k_i i - k_s y \tag{4.6}$$

where $k_i = 4ki_0 / s_0^2$ and $k_s = 4ki_0^2 / s_0^3$. This model is similar to that for an AMB [88] supporting a circular shaft with infinite radius. The resultant magnetic force is perpendicular to the target surface and does not act at an angle as it would with a circular shaft.

From Table 4.1, we can calculate the magnetic factors k_i and k_s, which are 41 N/Amp and -7.6×10^4 N/m respectively. The actuator force can be determined from equation (4.6).

Table 4.1 Parameters values of actuator

parameter	symbol	value	units
Cross section area of the air gap	A_a	25×15	mm^2
Number of turns in magnet coil	n	192	turns
Nominal air gap for actuator 1	s_0	0.67	mm
Nominal air gap for actuator 2	s_0	0.67	mm
Bias current	i_0	1.5	Amp

Copyright© by Chiang Mai University
All rights reserved

4.4 Instrumentation and Data Acquisition

An xPC Target computer system was used to digitally implement the controllers for the test system. The connections required for operation of the test system are shown in Figure 4.10. The xPC Target system consist of two computer units: (i) host computer and (ii) target computer. The host computer is used to compute, analyse and compile the control algorithms for the test system and also receive/transmit the data signals during operation. The target computer is used as a real-time processor to implement the control algorithm and/or monitor real-time input/output data. The input/output boards on the target computer are MM-16AT Diamond Analog Input and Ruby-MM-1612 Diamond Analog Output respectively. These boards are compatible with MATLAB® xPC toolbox in the host computer.

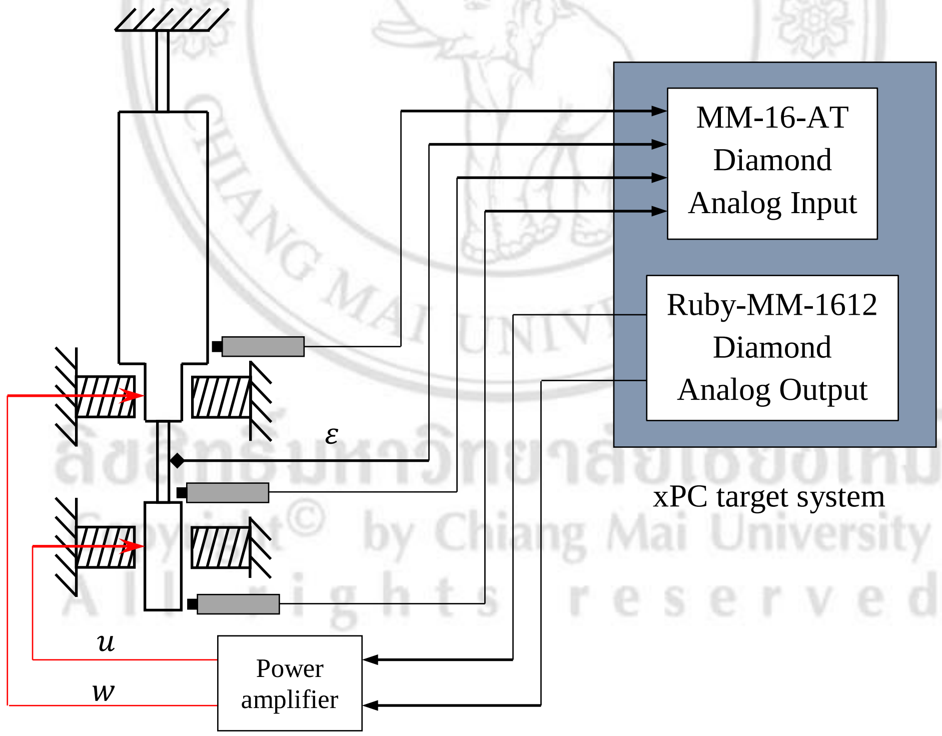

Figure 4.10 xPC Target system and test system connecting diagram

Copyright© by Chiang Mai University
All rights reserved

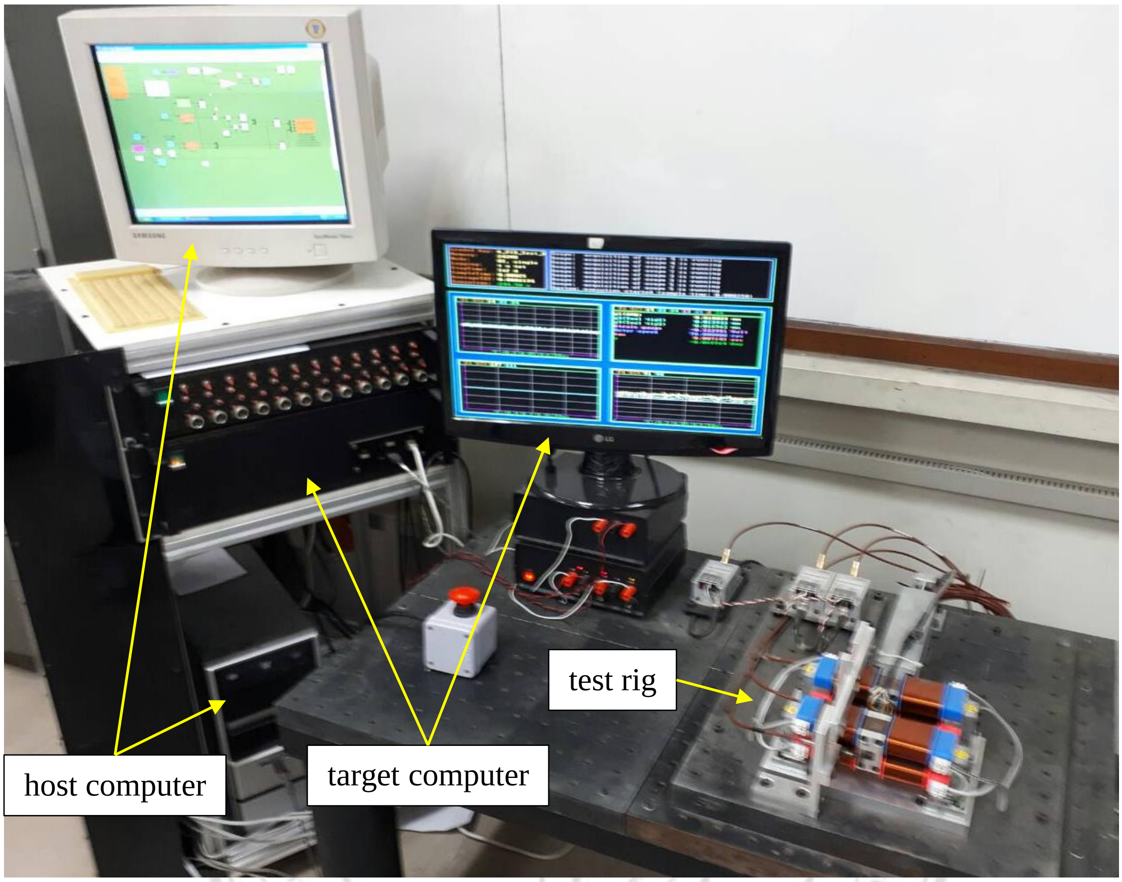

Figure 4.11 Test system and xPC target computer system

4.5 Stabilizing Local PD Control

This section describes the preliminary control set up for the test system based on PD feedback of displacements measured locally to the actuators (see Figure 4.13). Note that both actuators have a local PD feedback implementation but, as explained in Section 4.1, actuator 1 is used for vibration control and actuator 2 is used for the cutting force generation. Therefore, the description of the basic control for each actuator is given below.

Actuator 1: The PD controller for actuator 1 can be specified in the form

$$u_{PD} = k_i i - k_s y_a = k_i\left(-K_P y_a - K_D \frac{d(y_a)}{dt}\right) - k_s y_a \tag{4.7}$$

where K_P is the proportional feedback gain and K_D is the differential feedback gain. The displacement signal of the test system structure at actuator 1 (y_a) is obtained from the sensor 1 as shown in Figure 4.12. This signal was also used to calculate the velocity (derivative). Note that k_s has negative value and is the intrinsic property of the electromagnet which with controller, would have a destabilizing effect on the test structure. Thus, adjustment of the control gain K_P is first considered. From (4.7), for stabilizing the test system structure, the absolute value of K_P must be more than the absolute value of the negative stiffness: $|K_P| > |k_s|$. Then the derivative control gain K_D can be adjusted until the damping of the rigid body mode for the test system structure is suitable for operation. The suitable PD control gains were $K_P = 1.8|k_s|$ N/m and $K_D = 6$ Ns/m. Note that, the value of K_D highly influences the modal damping levels which tend to increase with increasing K_D. However, too high a value tends to reduce damping of the flexible mode. This will be explained further in Chapter 5.

Actuator 2: For this actuator, the main purpose of the local PD control is to cancel the negative stiffness of the actuator. Thus the proportional control gain K_{P2} should match the absolute negative stiffness, $|K_{P2}| \approx |k_s|$. In practice, it is difficult to determine the exact values of k_i and k_s. Therefore, we can adjust the value of K_{P2} and observe the vibration of the test system until it is close to the marginally stable operation. A small

ลิขสิทธิ์มหาวิทยาลัยเชียงใหม่
Copyright© by Chiang Mai University
All rights reserved

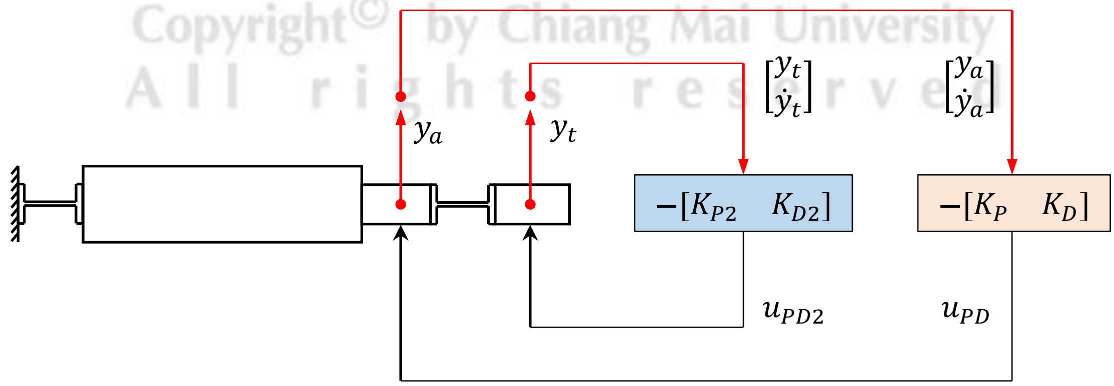

Figure 4.12 The preliminary stabilizing control scheme for the test system

non-zero value of K_{D2} is also required to compensate for some phase lag in the feedback control and achieve stable operation. In this case, the suitable PD control gains were $K_{P2} = 0.7|k_s|$ N/m and $K_{D2} = 1.7$ Ns/m.

4.6 Experimental Results with PD Feedback Control

To establish a baseline performance, preliminary test results with the local PD control were obtained by applying additional excitation forces through the actuators as shown in Figure 4.13. In this way the frequency response of the test system is obtained. The I/O signals for the test system can be represented by four transfer functions of frequency response resulting in the form

$$y_m = G_{test} f_{test} \tag{4.8}$$

where $y_m = [y_a \quad y_t]^T$ and $f_{test} = [f_1 \quad f_2]^T$. The transfer function matrix (under local PD feedback control) is

$$G_{test} = \begin{bmatrix} g_{y_a f_1}^{test} & g_{y_a f_2}^{test} \\ g_{y_t f_1}^{test} & g_{y_t f_2}^{test} \end{bmatrix}.$$

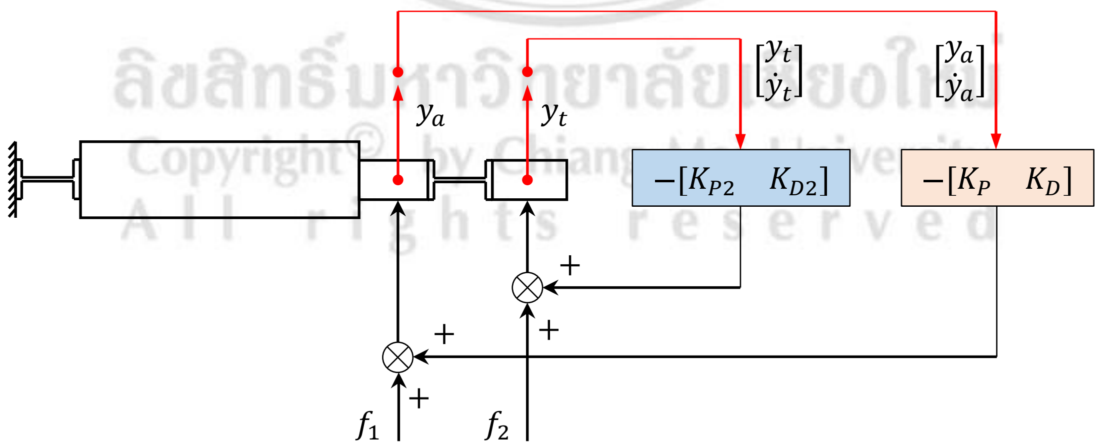

Figure 4.13 Control scheme for initial testing

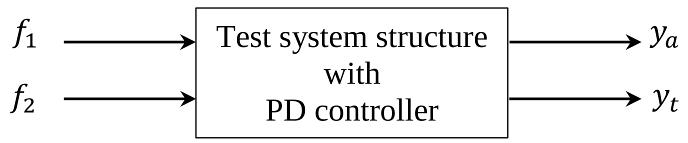

Figure 4.14 Frequency sweep testing inputs and output

By using frequency sweep testing method we determine the data of G_{test} according to the block diagram shown in Figure 4.14.

The frequency response results for the test system structure with PD control are shown in Figure 4.15. There are two main resonant frequencies: the low frequency mode (which involves 'rigid' body rotation) has the value $\omega_{n1} \approx 200$ rad/sec and the high frequency mode which involves significant bending of the end flexure has the value $\omega_{n2} \approx 546$ rad/sec, which we refer to as the *tool bending mode*.

Further experimental testing was performed with emulation of the cutting force applied through actuator 2. This allows us to obtain two main results which are (i) the cutting stability boundary (SLD) and (ii) the time response behaviour with the full simulation of the cutting force model.

The experiments were undertaken where the cutting force was realized by using the auxiliary actuator 2. Figure 4.16 shows the maximum depth-of-cut parameter for vibrational stability for the base-level PD control. To obtain the experimental boundary, the cutting force model was implemented using (2.5) with $h_m(t) = 0$, (as $h_m(t)$ acts as an additive disturbance and should not affect stability for linear operation). The value of the depth-of-cut parameter was gradually increased until an unstable growth in vibration occurred. This was repeated for a range of rotational speeds (time delay values). We can see that there is a clear repeating lobe pattern which is associated with the tool bending mode. Note that between the second and third lobe, the gap is cut by a competing lobe. This lobe is associated with the rigid body mode. This occurs because the value of the real part of the frequency response function $G(\mathrm{j}\omega)$ is similar for two different values of ω, i.e. when ω is close to rigid body mode frequency and when ω is close to the tool

ลิขสิทธิ์มหาวิทยาลัยเชียงใหม่
Copyright© by Chiang Mai University
All rights reserved

bending mode frequency [2]. We can observe these two resonant frequencies from the frequency response function $G_{y_t f_2}$ shown in Figure 4.15.

In the simulated cutting force testing, the tool was modelled as a two straight tooth (non-helical) square mill with diameter of 5 mm. The cut was performed with 30% radial immersion. For these conditions, the cut profile, as defined by the zero-vibration chip thickness $\left(h_m(t)\right)$ given by (2.3) has peak values of 0.28 mm, as shown in Figure 4.17. A rotational frequency of 16 Hz was simulated, for which the stability boundaries relate to the $N_c = 2$ cycle number. A detailed plot of the stability boundaries near to this operating point are shown in Figure 4.18.

The cutting force model (2.5) was implemented together with the PD controller, and was applied with selected values for the depth-of-cut parameter $\left(b_K = bK_{cut}\right)$. The time series data for system variables are shown in Figure 4.19. These tests involved sequential step increases in the depth-of-cut parameter b_K. The test results show step increases in vibration magnitude occur when the value of b_K is increased. Note that the value of b_K affects h_m as well as the feedback effect from the cutting dynamics. The onset of instability is consistent with the experimental stability lobe diagrams and is indicated by an exponential growth in cutting vibration. Note that the experiments were halted shortly after the onset of instability to prevent damage to the test system. The experimental results shown in this section provide a 'base level' performance under local PD control.

ลิขสิทธิ์มหาวิทยาลัยเชียงใหม่
Copyright© by Chiang Mai University
All rights reserved

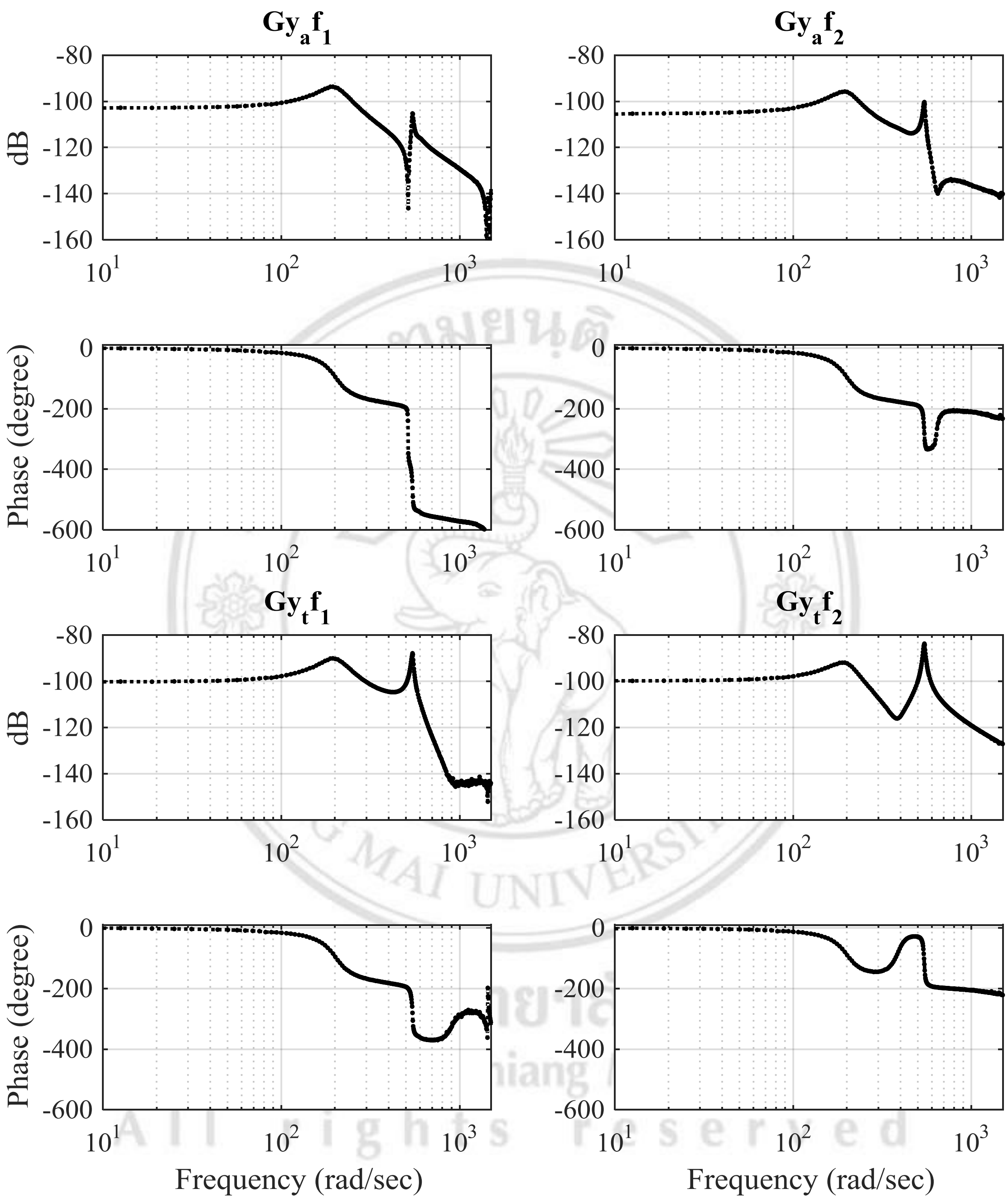

Figure 4.15 Frequency response of the test rig with PD controller

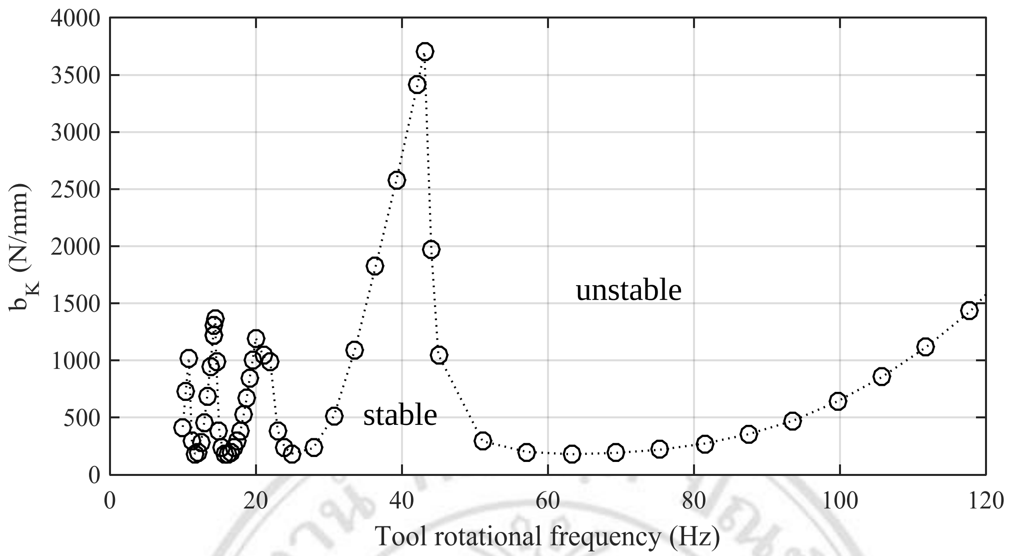

Figure 4.16 Stability regions from experiment with local PD control

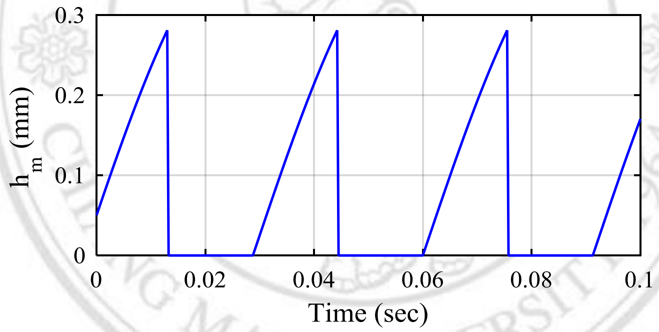

Figure 4.17 Mean chip thickness profile function used in cutting simulation

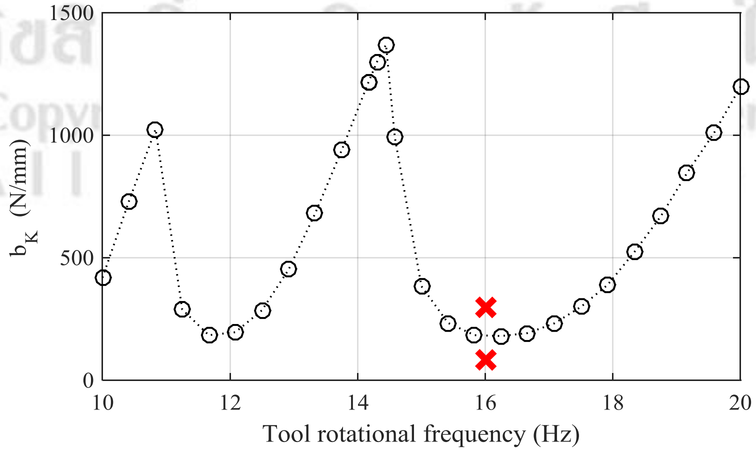

Figure 4.18 Close-up of stability boundary and selected rotational frequency for cutting simulations

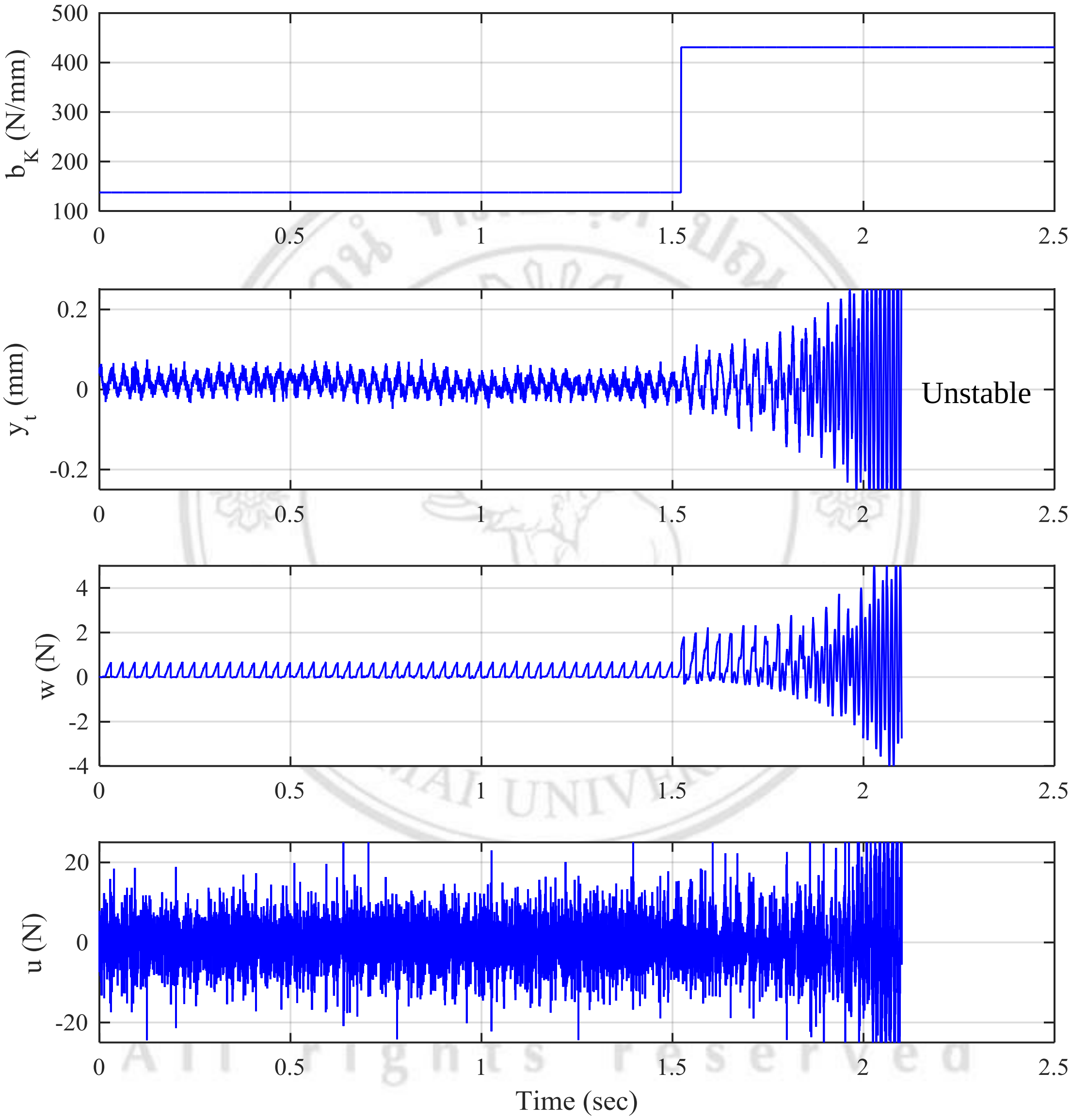

Figure 4.19 Cutting emulation on test system for 16 Hz rotational frequency

ลิขสิทธิ์มหาวิทยาลัยเชียงใหม่
Copyright© by Chiang Mai University
All rights reserved